

This is an Open Access document downloaded from ORCA, Cardiff University's institutional repository: <https://orca.cardiff.ac.uk/id/eprint/122468/>

This is the author's version of a work that was submitted to / accepted for publication.

Citation for final published version:

Pavliuk, Mariia V., Gutiérrez Álvarez, Sol, Hattori, Yocef, Messing, Maria E., Czaplak-Masztafiak, Joanna, Szlachetko, Jakub, Silva, Jose L., Araujo, Carlos Moyses, Fernandes, Daniel L. A., Lu, Li, Kiely, Christopher J., Abdellah, Mohamed, Nordlander, Peter and Sá, Jacinto 2019. Hydrated electron generation by excitation of copper localized surface plasmon resonance. *The Journal of Physical Chemistry Letters* 10 (8), pp. 1743-1749. 10.1021/acs.jpcclett.9b00792

Publishers page: <http://dx.doi.org/10.1021/acs.jpcclett.9b00792>

Please note:

Changes made as a result of publishing processes such as copy-editing, formatting and page numbers may not be reflected in this version. For the definitive version of this publication, please refer to the published source. You are advised to consult the publisher's version if you wish to cite this paper.

This version is being made available in accordance with publisher policies. See <http://orca.cf.ac.uk/policies.html> for usage policies. Copyright and moral rights for publications made available in ORCA are retained by the copyright holders.



Hydrated Electron Generation by Excitation of Copper Localized Surface Plasmon Resonance

Mariia V. Pavliuk,^{#,¶} Sol Gutierrez^{Alvarez,} Yocef Hattori,^{#,¶} Maria E. Messing,[†]
Joanna Czapla-Masztafiak,[‡] Jakub Szlachetko,^{‡,||} Jose L. Silva,[∇] Carlos Moyses Araujo,[∇]
Daniel L. A. Fernandes,^{*,#} Li Lu,[§] Christopher J. Kiely,[§] Mohamed Abdellah,^{*,#,*}
Peter Nordlander,[⊥] and Jacinto Sa^{*,#}

[#]Physical Chemistry Division, Department of Chemistry, Ångström Laboratory, Uppsala University, 75120 Uppsala, Sweden

[†]Solid State Physics and NanoLund, Lund University, Box 118, 22100 Lund, Sweden

[‡]Institute of Nuclear Physics, Polish Academy of Sciences, PL-31342 Krakow, Poland

^{||}Institute of Physical Chemistry, Polish Academy of Sciences, 01-224 Warsaw, Poland

[∇]Materials Theory Division, Department of Physics and Astronomy, Uppsala University, 75120 Uppsala, Sweden

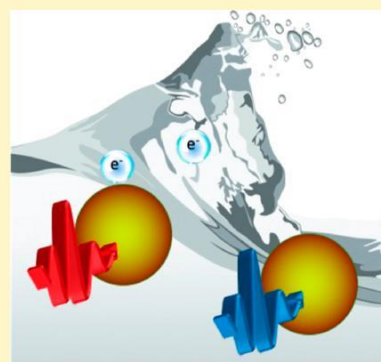
[§]Department of Materials Science and Engineering, Lehigh University, 5 East Packer Avenue, Bethlehem, Pennsylvania 18015, United States

^{*}Department of Chemistry, Qena Faculty of Science, South Valley University, 83523 Qena, Egypt

[⊥]Department of Physics, Rice University, 6100 South Main Street, Houston, Texas 77251-1892, United States

* Supporting Information

ABSTRACT: Hydrated electrons are important in radiation chemistry and charge-transfer reactions, with applications that include chemical damage of DNA, catalysis, and signaling. Conventionally, hydrated electrons are produced by pulsed radiolysis, sonolysis, two-ultraviolet-photon laser excitation of liquid water, or photodetachment of suitable electron donors. Here we report a method for the generation of hydrated electrons via single-visible-photon excitation of localized surface plasmon resonances (LSPRs) of supported sub-3 nm copper nanoparticles in contact with water. Only excitations at the LSPR maximum resulted in the formation of hydrated electrons, suggesting that plasmon excitation plays a crucial role in promoting electron transfer from the nanoparticle into the solution. The reactivity of the hydrated electrons was confirmed via proton reduction and concomitant H₂ evolution in the presence of a Ru/TiO₂ catalyst.



The nature of the hydrated electron is a long-standing scientific question. The first evidence of hydrated electrons dates back to 1808 when Humphry Davy observed a “beautiful metallic appearance” and “fine blue color” when potassium crystals were heated in the presence of ammonia vapor.¹ More than a century later, this effect would become understood as evidence for solvated electrons. As early as 1952, these species were suggested to be the primary radicals formed upon radiolysis of water,² which was demonstrated experimentally a decade later.³ Questions regarding the detailed structure of the hydrated electron persist.⁴ The initial consensus was that the hydrated electron occupies a quasi-spherical cavity in liquid water,^{5,6} i.e., a particle in a quasi-spherical solvent void, an idea contested by Larsen et al. in 2010.⁷ Their theoretical calculations suggested that a hydrated electron occupies a ~1 nm diameter region of enhanced water density. The structure of the hydrated electron remains a highly debated issue and has been the subject of recent review articles.^{4,8}

The interest in hydrated electrons is fueled by their potential applications. Electrons with kinetic energies in the 3–20 eV range can induce single- and double-strand breaking in DNA.⁹ Electrons with even lower energy (0.1–2.0 eV) can induce covalent bond cleavage in DNA,^{10–12} dissociative electron transfer to CCl₄,¹³ dechlorination of selected aliphatic and aromatic chlorides,¹⁴ as well as the reduction of ketones¹⁴ and molecular oxygen.¹⁵ This makes low-energy hydrated electrons attractive to the fields of medicinal therapy, catalysis, and signaling. However, the full exploitation of hydrated electrons in such applications demands more efficient approaches for their production, preferentially using visible or infrared light.

Hydrated electrons are conventionally generated by pulsed radiolysis,¹⁶ sonolysis,¹⁷ two-ultraviolet-photon laser excitation¹⁸ of liquid water, or photodetachment of suitable electron

donors.¹⁹ Hydrated electrons are commonly detected with transient absorption spectroscopy (TAS)^{20–23} and X-ray photoelectron spectroscopy.^{24,25} Reports on hydrated electron formation using visible photon excitation are scarce. Recently, Naumann et al.¹⁴ reported an elegant way to produce hydrated electrons in a mixture containing a ruthenium-based photo-catalyst and ascorbate dianions from vitamin C using multiphoton excitation events employing light in the green range of the visible electromagnetic spectrum. However, to our knowledge, hydrated electron production by single-photon excitation in the visible wavelength range has not yet been reported.

Hot carriers in plasmonic nanoparticles (NPs) can be generated both by direct excitation and, much more efficiently, by localized surface plasmon resonance (LSPR) excitation and decay.²⁶ The energy of the resulting electron-hole pair is determined by the incoming photon energy, but the energy distribution depends on the excitation process. Plasmon decay results in higher-energy (hot) electrons and (cold) holes just below the Fermi energy, while direct excitation typically results in colder electrons and hotter holes.²⁷ Both excitation mechanisms result in non-Fermi distributions of carriers that rapidly relax to a Fermi distribution predominantly through electron-electron scattering. The lifetimes of the hot carriers depend on their energy, ranging from ca. 1 ps for electrons ~ 0.5 eV above the Fermi energy to a few 100 fs for hot electrons with ~ 3 eV of energy.²⁸ For nanoscopic systems, such as the sub-3 nm Cu NPs described here, quantum size effects play an important role for the plasmon, limiting its collection efficiency (plasmonicity) as well as introducing a blue shift and a broadening with respect to the LSPR of larger NPs.²⁹ Illumination around the plasmon energy at ~ 400 nm will generate hot electrons both from plasmon decay (extending up to 3 eV above the Fermi energy) and from direct excitation of interband transitions extending to around 0.7 eV above the Fermi level.³⁰ With a Cu work function of ~ 4.5 eV and a solvated electron binding energy of $\sim .3$ eV,¹⁸ eV, hot electrons with energies higher than ~ 1.2 eV above the Fermi level could in principle transfer into a hydrated electron state. Such electrons are readily produced via LSPR excitation. The effectiveness of this process will be governed by the NP size as it defines light absorption efficiency, plasmon strength, and LSPR lifetime.^{31,32}

In this Letter, it is shown that hydrated electrons can be produced via visible light excitation of the LSPR in Cu NPs. Hydrated electrons were observed only upon excitation at the LSPR absorption maximum, confirming that only LSPR-induced hot electrons possess sufficient energy to be ejected from the Cu NPs (Figure 1). The photoredox capabilities of the hydrated electrons were confirmed in a catalytic proton reduction reaction, leading to the evolution of molecular hydrogen on an adjacent Ru/TiO₂ NP species.

An aqueous suspension of Cu NPs was synthesized via chemical reduction of CuSO₄ with ascorbate/ascorbic acid with 5% sodium ascorbate at pH 5–7 in the presence of polyethylenimine in a microfluidic reactor³³ (see the Supporting Information (SI) for full experimental details). Polyethylenimine was selected because it is an effective capping agent for stabilizing Cu NPs in the metallic state while simultaneously restricting their growth.³⁴

The Cu NPs mean particle size was evaluated by dynamic light scattering (DLS) and estimated to be 2 nm ($N \approx 355$ atoms) (Figure S1). The Cu NPs were molecularly grafted

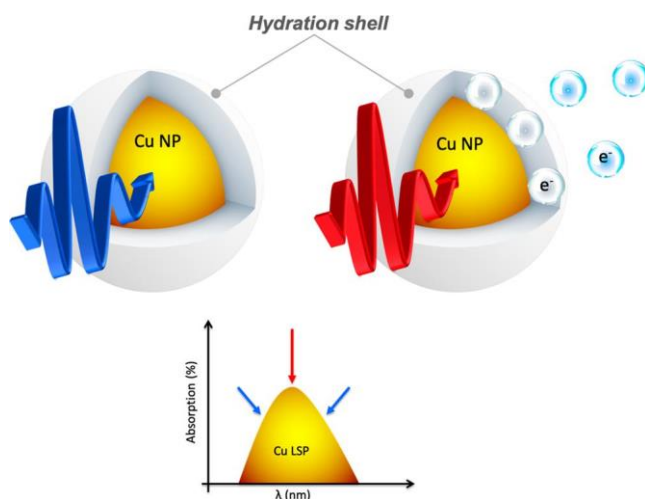


Figure 1. Schematic representation of hydrated electron formation due to localized surface plasmon excitation of copper NPs. Solvation and ejection of electrons only occur when the Cu NPs are excited at the LSPR maximum.

onto TiO₂ anatase with β -alanine and imaged by high-resolution transmission electron microscopy (HRTEM) (Figure 2A). Representative phase contrast images of the

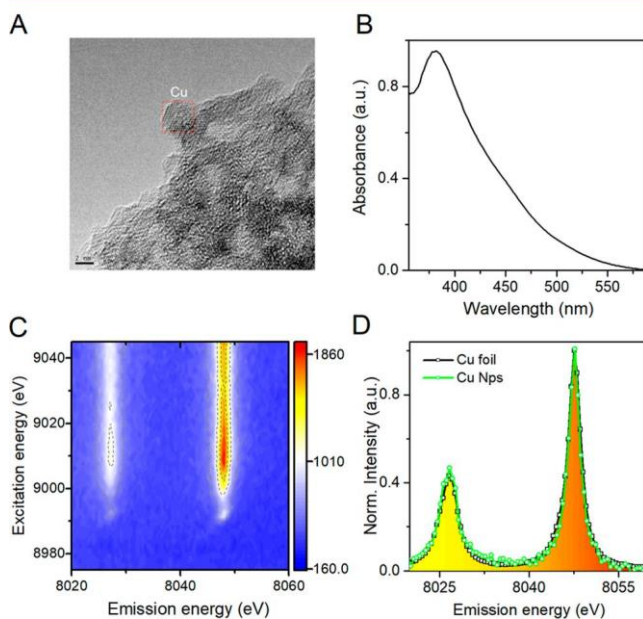


Figure 2. Characterization of Cu NPs used in this study. (A) Representative HRTEM micrograph of Cu NPs on TiO₂ anatase; (B) UV-visible spectrum of Cu NPs after synthesis showing the characteristic plasmon resonance absorption; (C) resonant X-ray emission spectroscopy (RXES) map of the Cu NPs measured around the Cu K-edge; and (D) K α -XES spectra for Cu NPs and a reference Cu metal foil extracted from RXES via a horizontal cut at an excitation energy of 9050 eV.

sample (Figure S2) show copper particles, typically in the 3–4 nm size range, supported on agglomerates of 2–3 nm TiO₂ particles. The inset FFTs represent the characteristic spacing and interplanar angles of the lattice fringes in the highlighted regions. The fast Fourier transfer (FFT) from Figure S2A,B closely correspond to the [001] and [110] projections, respectively, of the cubic Cu₂O structure. No good match

was found in these regions corresponding to f.c.c. Cu, monoclinic CuO, or the rutile or anatase phases of TiO₂. During sample preparation, the colloidal sample was deposited onto a holey carbon TEM grid and the solvent allowed to evaporate before insertion into the electron microscope. It is highly likely that during this aerobic transfer process the ultrasmall Cu NPs were oxidized to Cu₂O. Assuming this to be the case and considering the expected volume expansion that occurs upon oxidation, the original size of the nonoxidized Cu crystallites was estimated to be 2–3 nm, which is consistent with the DLS analysis.

The optical absorption spectrum (Figure 2B) from the colloidal Cu NPs has a clear peak centered at ~395 nm (~3.1 eV) that can be ascribed to the LSPR. The background signal relates to the absorption of polyethylenimine.³⁵ The rather low intensity of the plasmon band is expected based on the quantum size effects that lead to the formation of discrete quantized energy states, in contrast to band formation in larger particles.³²

The oxidation state of the Cu NPs under aerobic conditions was assessed by resonant X-ray emission spectroscopy (RXES, Figure 2C) and compared with a copper foil standard. The RXES map was identical to that of the metallic foil (see SI Figure S3), suggesting that NPs have a metallic character. This is confirmed by analysis of the K α -XES spectra (Figure 2D) extracted from a RXES map at a 9050 eV excitation energy and high-resolution X-ray absorption spectroscopy (HR-XAS) (Figures S3–S5), which shows no significant energy shift or broadening of the K α emission peak and no significant variation in the HR-XAS inflection point. Note that a 0.13 eV spectral shift should be expected in the K α emission profile if the sample were oxidized.³⁶ It is worth emphasizing that RXES measurements were performed directly on the Cu NPs 2 months after their synthesis, which confirms the effectiveness of the branched polyethylenimine ligands for stabilization and protection against oxidation. The findings were further substantiated by the absence of characteristic Raman peaks for Cu₂O or CuO (Figure S6). Note that the lack of signal is not related to a low-concentration effect because peaks associated with the TiO₂ anatase NPs that are present in a similar concentration are clearly detected by Raman spectroscopy (Figure S6).

The formation of hydrated electrons was evaluated with ultrafast TAS. The excitation wavelength was varied across the Cu NPs LSPR, and the photoinduced changes were probed between 350 and 800 nm. In the case of NPs, the heating of the electron gas (LSPR excitation) leads to spectral broadening of the surface plasmon absorption,^{30,37,38} resulting in transient bleaching at the center of the plasmon band maximum and two positive absorption wings at lower and higher energies (known as “winglets”) in the difference spectrum.^{30,38,39}

Figure 3A shows the two-dimensional color map of the temporal evolution of the surface plasmon resonance of Cu excited at 398 nm, i.e., excitation at the maximum of the LSPR absorption band. The transient signal shows the expected “bleaching” of the LSPR absorption band and a winglet band (positive transient absorption signal) centered at 480 nm.^{30,38,39} The winglet band at higher energies (i.e., shorter wavelength) was not observable due to the limited wavelength range of the probe light.

Analysis of the transient behavior of the winglet signal provides information about copper plasmonic relaxation dynamics (Figure 3B). The kinetic trace extracted at 500 nm

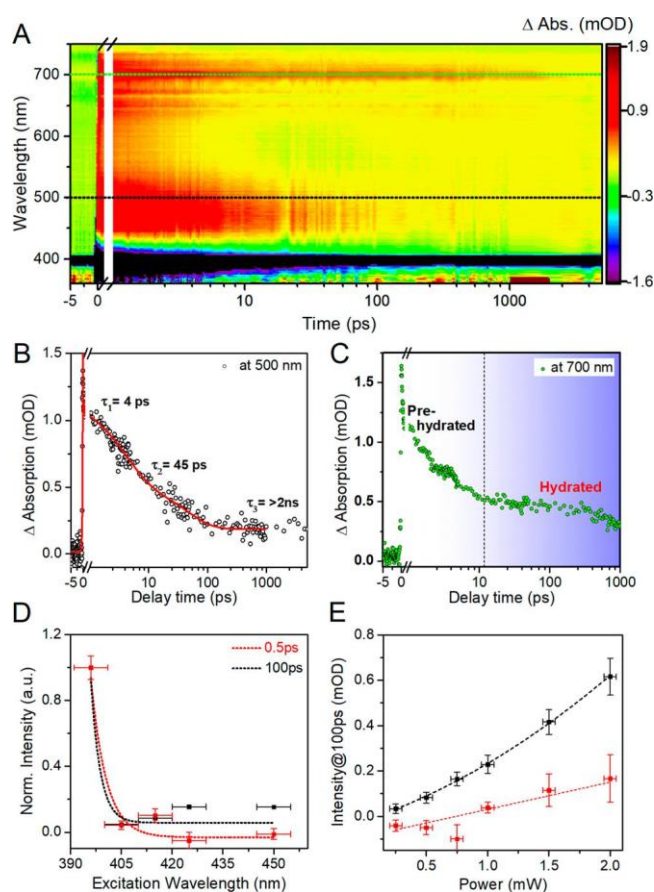


Figure 3. Ultrafast TAS analysis of Cu NPs. (A) Two-dimensional color map of the temporal evolution of the surface plasmon resonance of Cu excited at 398 nm; (B) kinetic trace extracted at 500 nm depicting the signal decay of positive absorption induced by plasmon excitation (“winglets”); (C) kinetic trace extracted at 700 nm depicting the signal ascribed to hydrated electrons, with black dashed line illustrating the time regime where prehydrated and hydrated electrons coexist; after 10 ps, the signal can be associated with only hydrated electrons; (D) normalized signal intensity at 690–710 nm as a function of excitation wavelength at two distinct times, namely, 0.5 ps (prehydrated + hydrated electrons) and 100 ps (hydrated electrons only); and (E) laser power dependence of the hydrated electron and winglet signals (intensities extracted at 100 ps).

(isolated winglet signal) was fitted with a rising component and three-exponential decay functions. The rising component was estimated to be around 400 fs, which is significantly longer than the instrumental resolution (~150 fs) and consequently must be assigned to electron–electron scattering.²⁸ In Fermi liquid theory, the lifetime of an excited electron is proportional to its energy relative to the Fermi level. Using the measured lifetime, one estimates that the hottest electrons have energies at least 0.7 eV above the Cu Fermi level.³⁰ The kinetic trace was fitted with two major exponential decay curves with characteristic lifetimes of 4 and 45 ps and a smaller long-lived component (>2 ns). By comparison to published results,³⁹ the fastest component was ascribed to electron–phonon scattering, while the 45 ps decay feature relates to phonon–phonon relaxation. The longest-lived component is a minor contribution and consequently is difficult to assign categorically, but we suspect that it is associated with phonon–solvent relaxation.³⁹

Careful analysis of the two-dimensional color map (Figure 3A) reveals a long-lived broad absorption signal starting at 600

nm with a maximum at $\sim 700\text{--}720$ nm, which cannot be assigned to any of the components from the Cu NPs. Similar transient signals have been observed upon excitation of the LSPR in Ag NPs⁴⁰ and differ only in their lifetimes. In the case of Ag, the signal was short-lived, decaying completely within 50–70 ps.⁴¹ The authors assigned it to solvated electrons on the metallic surface or prehydrated electrons because their lifetime was too short for the formation of fully hydrated electrons, which typically takes $\sim 10^{-11}$ s.^{4,16}

Analysis of the kinetic trace extracted at 700 nm revealed two distinct regions, namely, a fast-decaying component (ca. 3 ps) accounting for roughly 70% of the signal and a long-lived component that barely decayed over the experimental delay line (ca. 5 ns). The faster component was assigned to prehydrated electrons on the Cu NP surface, while the long-lived component was associated with hydrated electrons.^{21,41} Note that hydrated electrons can survive up to hundreds of μs (in neutral water at low concentrations).^{16,42}

As discussed, only the hottest electrons, which are formed for resonant excitation of the LSPR, carry sufficient energy to transfer into a hydrated state. Consequently, one should expect a decrease in hydrated electron formation when the excitation wavelength is detuned from the Cu LSPR maximum. Figure 3D shows the signal intensity in the 690–710 nm region as a function of excitation wavelength (390–450 nm) at two distinct times, namely, at 0.5 (prehydrated + hydrated electrons) and at 100 ps (hydrated electrons only). Indeed, once the excitation wavelength deviates from the LSPR maximum, the population of prehydrated and hydrated electrons rapidly decreases nearly to zero, confirming that only the peak of LSPR excitation in Cu NPs can yield electrons with sufficient energy to create hydrated electrons.^{26,27}

Further corroborating evidence that the hydrated electrons are due to the excitation of the Cu NPs LSPR and subsequent hot carrier generation can be found in the signal laser power dependence (Figure 3E). Quadratic behavior of the hydrated electron signal intensity versus the laser power is perceptible, which contrasts with the linear dependence for the winglet intensity versus the laser power. Superlinear power dependences of rates and intensities are characteristic of plasmon-induced hot carrier processes.⁴³ The hot carrier distribution is strongly affected by electron–electron scattering, with an average energy that increases with incident power when the time interval between subsequent photons becomes smaller than the lifetimes of the hot carriers.²⁸

To explore the possible use of hydrated electrons in photocatalysis, we carried out the following experiment. Plasmonic hot electrons can be transferred to acceptors such as semiconductors.⁴⁴ The ensemble plasmonic/semiconductor entity is characterized by an energy barrier (Schottky barrier), which can be accurately estimated. Thus, in order to inject electrons into the semiconductor conduction band, they must have a higher energy than the Schottky barrier height. The main limitation with this approach is that once the plasmonic nanostructure comes into contact with the surface of the semiconductor, band bending occurs. To prevent that from happening, one must keep the two structures physically separated in space but linked in some way so that one can minimize electron energy loss and promote electron transfer.

Density functional theory (DFT) was used to estimate the minimum spatial distance required between Cu NPs and TiO₂ to avoid band bending. Figure 4A,B shows the changes in the total (DOS) and projected density of states (pDOS) as a

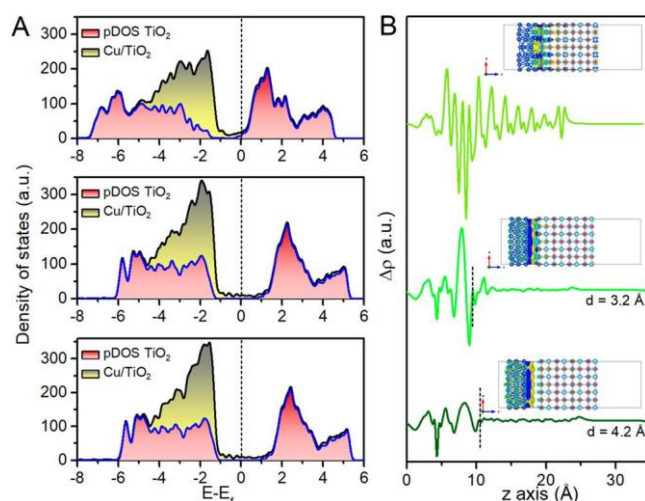


Figure 4. DFT calculations of the total pDOS for Cu(111)|TiO₂(100) anatase (A) of the intimate junction (top panel), the heterostructure with a fixed distance of 3.2 Å between the slabs (middle panel), and a fixed distance of 4.2 Å between the slabs (bottom panel) and (B) of the planar average electron density difference along the [001] direction (perpendicular to the surfaces) for the same three situations in (A), with the inset showing the atomic positions.

function of the distance between the TiO₂(100) and Cu(111) slabs. When the two the slabs are in direct contact, they form chemical bonds (see the optimized structure in the Figure 4B inset). A comparison between the total DOS of Cu(111)|TiO₂(100) and the one projected on the TiO₂ and on Cu(111) shows that this interface has the profile of an ohmic contact with no Schottky barrier. This is also evident in Figure 4B, where the planar average electron density difference along the [001] direction (perpendicular to the surfaces) is presented.

In contrast, when the Cu(111) and TiO₂(001) surfaces are separated by 3.2 Å nm, a sizable Schottky barrier of 0.69 eV can be calculated from the pDOS. An even larger Schottky barrier of 0.88 eV is found for a longer separation of 4.2 Å, as shown in Figure 4A (lower panel). The larger separation reduces the interaction and hybridization between the donor and acceptor states and increases the Schottky barrier height, leading to a higher resistance for electron transfer. Additionally, the results indicate that the valence charge density readjusts in the interface region and a dipole moment is generated to minimize the system energy from 6.0 to 10.5 Å. As the distance between the donor and acceptor states increases, a weaker dipole moment and stronger Schottky barrier height in the interface region are observed.

Our DFT calculations estimated a 0.88 eV barrier if the two structures were kept apart by about 4.2 Å. Thus, the Cu NPs were molecularly linked to a TiO₂ anatase semiconductor support via a nonconductive linker (β -alanine) by self-assembly, as reported elsewhere.⁴⁵ The molecular linker was chosen to create an optimal distance between the electron donor (Cu NPs) and acceptor (TiO₂) sites of ca. 4–5 Å and preserve the Schottky barrier as estimated by DFT.

Electron injection into the TiO₂ conduction band was followed by ultrafast transient infrared absorption spectroscopy (TIRAS).⁴⁶ Electron injection into a semiconductor results in mid-IR absorption originating from the free charge carriers in the conduction band. Figure 5A shows a kinetic trace extracted

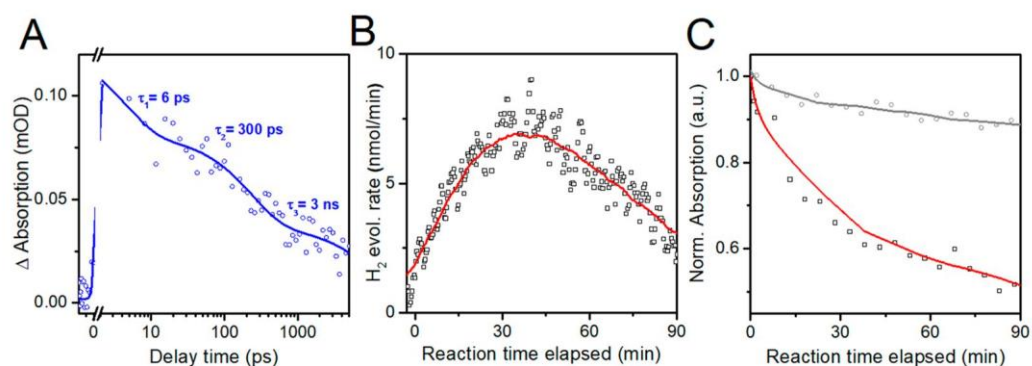


Figure 5. Electron transfer dynamics and photocatalysis. (A) Ultrafast transient infrared absorption spectroscopy (TIRAS) kinetic traces associated with electron injection into the TiO₂ conduction band after plasmon excitation at 405 nm; (B) hydrogen evolution profile as a function of reaction time upon CW laser excitation at 405 nm for the complete photosystem (Cu NPs linked with β -alanine to TiO₂ with Ru NPs co-catalyst); and (C) methylene blue photo-oxidation conversion profile reaction time upon CW laser excitation at 405 nm. (red trace) Cu NPs linked with β -alanine to TiO₂ with Ru NPs and (black trace) blank experiment with all components present except Cu NPs.

at 1950 cm⁻¹ from the injected electrons. A significantly larger signal and faster injection were observed when β -alanine was replaced by *p*-aminobenzoic acid (Figure S8A), a conductive molecular linker with similar length.

The injected electrons are rather long-lived, with a 30–40% fraction surviving more than 3 ns, which makes them suitable for photocatalysis. As a suitable photocatalytic test reaction, we chose to investigate H₂ evolution. To increase the H₂ evolution rate, ruthenium NPs were deposited onto TiO₂ to act as a co-catalyst. Figure S9 shows HAADF images of the Ru spatial and size distribution on the TiO₂ support.⁴⁵ TIRAS measurements confirmed fast transfer of the injected electrons into Ru NPs (Figure S8B).

H₂ evolution from Ru NPs and methylene blue oxidation on Cu NPs are shown in Figure 5B,C, respectively. Starting with H₂ evolution, it is clear from the data in Figure 5B that the injected hydrated electrons are indeed able to catalyze proton reduction on the Ru NPs. Note that reaction with the same Ru/TiO₂ system in the absence of Cu NPs did not yield any hydrogen as expected. Considering that the free electron density in Cu is $8.47 \times 10^{28} \text{ m}^{-3}$ and assuming an average particle size of 3 nm, there are ca. 4.0×10^{17} electrons per mL available to react. The steady-state hydrogen production rate (ca. 5 nmol H₂ per min per gram of catalyst) requires ca. 6.0×10^{15} electrons/min, which would exhaust the accessible electrons in less than 20 min. To prevent this from happening, methylene blue was introduced. Methylene blue oxidation is a one-electron process with a rather low redox potential, (i.e., a photo-oxidation process with a high rate of reaction). Additionally, methylene blue depletion can be dynamically monitored using UV-vis spectroscopy. Figure 5C shows that indeed the holes left behind in the Cu NPs can be refilled through methylene blue oxidation, prolonging the H₂ evolution beyond 20 min. Note that the use of very small (sub-3 nm) Cu NPs, while challenging due to their notorious instability in aqueous media and aerobic conditions,⁴⁷ guarantees a high reaction rate in methylene blue oxidation (i.e., allowing effective refilling of the photogenerated hole) due to their large surface area. This is corroborated by the fact that once the one electron oxidation substrate is nearly depleted the system starts to deactivate because the subsequent reactions are more difficult to carry out due to the energetics involved.

In summary, we have shown that LSPR excitation and hot carrier generation in Cu NPs in contact with water can result in the efficient production of hydrated electrons. Some of the electrons possess an energy of at least 0.88 eV, as confirmed by theoretical prediction and experimental observations, making them highly reactive. We show that the hydrated electrons can catalyze proton reduction to molecular hydrogen by trans-ferring them into an adjacent catalyst (TiO₂ with Ru NPs) via a suitable linker molecule. Our studies suggest that hydrated electrons may be of significant use as intermediate acceptors in plasmon-enhanced photocatalysis and potentially in DNA covalent bond disruption based on their high energy. The small size of the Cu NPs might facilitate their uptake by cells, which could offer possibilities for novel nanoscale therapeutic applications.

■ ASSOCIATED CONTENT

*

Materials and methods, theoretical calculations, information on hydrogen evolution experiments, figures representing DLS measurements on the Cu NPs colloid, profile-view phase contrast TEM images of Cu-containing NPs supported on TiO₂, RXES of Cu NPs and Cu foil, HR-XAS spectra, nonresonant Raman spectra, representation of the nanohybrid system used for the production of molecular hydrogen, ultrafast transient infrared absorption spectroscopy kinetic measurements, and representative high-angle annular dark field (HAADF) STEM image of Ru on TiO₂ (PDF)

■ AUTHOR INFORMATION

Corresponding Authors

*E-mail: jacinto.sa@kemi.uu.se.

*E-mail: daniel.fernandes@angstrom.se.

*E-mail: mohamed.qenawy@kemi.uu.se.

ORCID

Joanna Czapla-Masztafiak: 0000-0001-7706-0296

Carlos Moyses Araujo: 0000-0001-5192-0016

Li Lu: 0000-0002-6688-1176

Mohamed Abdellah: 0000-0002-6875-5886

Peter Nordlander: 0000-0002-1633-2937

Jacinto Sa: 0000-0003-2124-9510

Author Contributions

M.V.P. and S.G.A. contributed equally. J. Sa proposed the concept and directed the research. M.V.P., S.G.A., D.L.A.F., C.M.A., M.A., P.N., and J. Sa designed the experiments. M.V.P., S.G.A., D.L.A.F., M.A., Y.H., J.C.-M., J. Szlachetko, and J. Sa carried out the experiments, except electron microscopy. C.J.K., L.L., and M.E.M. performed all electron microscopy measurements and analysis. J.L.S. and C.M.A. performed the theoretical calculations. M.V.P. and J. Sa prepared the figures. J. Sa wrote the main manuscript text. All authors contributed to the discussion on experimental data and data analysis and reviewed the manuscript.

Notes

The authors declare no competing financial interest.

ACKNOWLEDGMENTS

The authors would like to thank Uppsala University, Stiftelsen Olle Engkvist Byggmastare, and the Swedish Research Council for financial support. We would like to thank Shmector.com for permission to use the background of Figure S8. C.M.A. would like to thank STandUp collaboration for financial support. The computational studies were performed using resources provided by the Swedish National Infrastructure for Computing (SNIC) at the PDC Center for High-Performance Computing and at the National Supercomputer Centre at Linköping University (NSC). P.N. acknowledges support from the Robert A. Welch foundation under Grant C-1222.

ABBREVIATIONS

LSPR, localized surface plasmon resonance; NPs, nanoparticles; HRTEM, high-resolution transmission electron microscopy; HAADF-STEM, high-angle annular dark field scanning transmission electron microscopy; RXES, resonant X-ray emission spectroscopy; DLS, dynamic light scattering; HR-XAS, high-resolution X-ray absorption spectroscopy; TAS, transient absorption spectroscopy.

REFERENCES

- (1) Thomas, J. M.; Edwards, P. P.; Kuznetsov, V. L. Sir Humphry Davy: Boundless Chemist, Physicist, Poet and Man of Action. *ChemPhysChem* 2008, 9, 59–66.
- (2) Stein, G. Some aspects of the radiation chemistry of organic solutes. *Discuss. Faraday Soc.* 1952, 12, 227–234.
- (3) Hart, E. J.; Boag, J. W. Absorption spectrum of the hydrated electron in water and in aqueous solutions. *J. Am. Chem. Soc.* 1962, 84, 4090–4095.
- (4) Herbert, J. M.; Coons, M. P. The Hydrated Electron. *Annu. Rev. Phys. Chem.* 2017, 68, 447–472.
- (5) Ogg, R. A., Jr. Physical interactions of electrons with liquid dielectric media. The properties of metal-ammonia solutions. *Phys. Rev.* 1946, 69, 668–669.
- (6) Jortner, J.; Rice, S. A. Theoretical studies of solvated electrons. *Adv. Chem. Ser.* 1965, 50, 7–26.
- (7) Larsen, R. E.; Glover, W. J.; Schwartz, B. J. Does the hydrated electron occupy a cavity? *Science* 2010, 329, 65–69.
- (8) Casey, J. R.; Kahros, A.; Schwartz, B. J. To be or not to be in a cavity: the hydrated electron dilemma. *J. Phys. Chem. B* 2013, 117, 14173–14182.
- (9) Boudaïffa, B.; Cloutier, P.; Hunting, D.; Huels, M. A.; Saeche, L. Resonance formation of DNA strand breaks by low-energy (3–20 eV) electrons. *Science* 2000, 287, 1658–1660.

- (10) Wang, C.-R.; Nguyen, J.; Lu, Q.-B. Bond breaks of nucleotides by dissociative electron transfer of non-equilibrium pre-hydrated electrons: A new molecular mechanism for reductive DNA damage. *J. Am. Chem. Soc.* 2009, 131, 11320–11322.
- (11) Simons, J. How do low-energy (0.1–20 eV) electrons cause DNA strand breaks? *Acc. Chem. Res.* 2006, 39, 772–779.
- (12) Sanche, L. Beyond radical thinking. *Nature* 2009, 461, 358–359.
- (13) Wang, C.-R.; Drew, K.; Luo, T.; Lu, M.-J.; Lu, Q.-B. Resonant dissociative electron transfer of the pre-solvated electron to CCl₄ in liquid: Direct observation and lifetimes of the CCl₄⁻ transition state. *J. Chem. Phys.* 2008, 128, No. 041102.
- (14) Naumann, R.; Kerzig, C.; Goetz, M. Laboratory-scale photo-redox catalysis using hydrated electrons sustainably generated with a single green laser. *Chem. Sci.* 2017, 8, 7510–7520.
- (15) Rasburn, E. J.; Michaels, H. B. On the reaction of hydrated electrons with oxygen. *Radiat. Phys. Chem.* 1977, 10, 289–290.
- (16) Walker, D. C. The hydrated electron. *Q. Rev., Chem. Soc.* 1967, 21, 79–108.
- (17) Dharmarathne, L.; Ashokkumar, M.; Grieser, F. On the generation of hydrated electron during sonolysis of aqueous solutions. *J. Phys. Chem. A* 2013, 117, 2409–2424.
- (18) Siefertmann, K. R.; Liu, Y.; Lugovoy, E.; Link, O.; Faubel, M.; Buck, U.; Winter, B.; Abel, B. Binding energies, lifetimes and implications of bulk and interface solvated electrons in water. *Nat. Chem.* 2010, 2, 274–279.
- (19) Martini, I. B.; Barthel, E. R.; Schwartz, B. J. Mechanisms of the ultrafast production and recombination of solvated electrons in weakly polar fluids: comparison of multiphoton ionization and detachment via the charge-transfer-to-solvent transition of Na⁺ in THF. *J. Chem. Phys.* 2000, 113, 11245–11257.
- (20) Kimura, Y.; Alfano, J. C.; Walhout, P. K.; Barbara, P. F. Ultrafast transient absorption spectroscopy of the solvated electron in water. *J. Phys. Chem.* 1994, 98, 3450–3458.
- (21) Kummrow, A.; Emde, M. F.; Baltuska, A.; Pshenichnikov, M. S.; Wiersma, D. A. Wave packet dynamics in ultrafast spectroscopy of the hydrated electron. *J. Phys. Chem. A* 1998, 102, 4172–4176.
- (22) Turi, L.; Rossky, P. J. Theoretical studies of spectroscopy and dynamics of hydrated electrons. *Chem. Rev.* 2012, 112, 5641–5674.
- (23) Vilchiz, V. H.; Kloepfer, J. A.; Germaine, A. C.; Lenchenkov, V. A.; Bradforth, S. E. Map for the relaxation dynamics of hot photoelectrons injected into liquid water via anion threshold photodetachment and above threshold solvent ionization. *J. Phys. Chem. A* 2001, 105, 1711–1723.
- (24) Luckhaus, D.; Yamamoto, Y.-I.; Suzuki, T.; Signorell, R. Genuine binding energy of the hydrated electron. *Sci. Adv.* 2017, 3, No. e1603224.
- (25) Elkins, M. H.; Williams, H. L.; Shreve, A. T.; Neumark, D. M. Relaxation mechanism of the hydrated electron. *Science* 2013, 342, 1496–1499.
- (26) Manjavacas, A.; Liu, J. G.; Kulkarni, V.; Nordlander, P. Plasmon-induced hot carriers in metallic nanoparticles. *ACS Nano* 2014, 8, 7630–7638.
- (27) Zheng, B. Y.; Zhao, H.; Manjavacas, A.; McClain, M.; Nordlander, P.; Halas, N. J. Distinguishing between plasmon-induced and photoexcited carriers in a device geometry. *Nat. Commun.* 2015, 6, 7797.
- (28) Liu, J. G.; Zhang, H.; Link, S.; Nordlander, P. Relaxation of plasmon-induced hot carriers. *ACS Photonics* 2018, 5, 2584–2595.
- (29) Zhang, R.; Bursi, L.; Cox, J. D.; Cui, Y.; Krauter, C. M.; Alabastri, A.; Manjavacas, A.; Calzolari, A.; Corni, S.; Molinari, E.; et al. How To identify plasmons from the optical response of nanostructures. *ACS Nano* 2017, 11, 7321–7335.
- (30) Hodak, J. H.; Martini, I.; Hartland, G. V. Spectroscopy and dynamics of nanometer-sized noble metal particles. *J. Phys. Chem. B* 1998, 102, 6958–6957.
- (31) Kreibig, U. Anomalous frequency and temperature dependence of the optical absorption of small gold nanoparticles. *J. Phys. Colloques* 1977, 38 (C2), C2-97–C2-103.

- (32) Logunov, S. L.; Ahmadi, T. S.; El-Sayed, M. A.; Khoury, J. T.; Whetten, R. L. Electron dynamics of passivated gold nanocrystals probed by sub-picosecond transient absorption spectroscopy. *J. Phys. Chem. B* 1997, **101**, 3713–3719.
- (33) Fernandes, D. L. A.; Paun, C.; Pavliuk, M. V.; Fernandes, A. B.; Bastos, E. L.; Sa, J. Green microfluidic synthesis of monodisperse silver nanoparticles via genetic algorithm optimization. *RSC Adv.* 2016, **6**, 95693–95697.
- (34) Ershov, B. G. Colloidal copper in aqueous solution: radiation-chemical reduction, mechanism of formation, and properties. *Russ. Chem. Bull.* 1994, **43**, 16–21.
- (35) Jia, J.; Wu, A.; Luan, S. Spectrometry recognition of polyethyleneimine towards heavy metal ions. *Colloids Surf., A* 2014, **449**, 1–7.
- (36) Kawai, J.; Nihei, Y.; Fujinami, M.; Higashi, Y.; Fukushima, S.; Gohshi, Y. Charge transfer effects on the chemical shift and the line width of the Cu K α X-ray fluorescence spectra copper oxides. *Solid State Commun.* 1989, **70**, 567–571.
- (37) Link, S.; El-Sayed, M. A. Spectral properties and relaxation dynamics of surface plasmon electronic oscillations in gold and silver nanodots and nanorods. *J. Phys. Chem. B* 1999, **103**, 8410–8426.
- (38) Aiboushev, A.; Gostev, F.; Shelaev, I.; Kostrov, A.; Museur, L.; Traore, M.; Sarkisov, O.; Nadochenko, V.; Kanaev, A. Spectral properties of the surface plasmon resonance and electron injection from gold nanoparticles to TiO₂ mesoporous film: femtosecond study. *Photochem. Photobiol. Sci.* 2013, **12**, 631–637.
- (39) Ahmadi, T.; Logunov, S. L.; El-Sayed, M. A. Picosecond dynamics of colloidal gold nanoparticles. *J. Phys. Chem.* 1996, **100**, 8053–8056.
- (40) Roberti, T. W.; Smith, B. A.; Zhang, J. Z. Ultrafast electron dynamics at the liquid-metal interface: femtosecond studies using surface plasmons in the aqueous silver colloid. *J. Chem. Phys.* 1995, **102**, 3860–3866.
- (41) Boag, J. W.; Hart, E. J. Absorption spectra in irradiated water and some solution-absorption spectra of hydrated electrons. *Nature* 1963, **197**, 45–47.
- (42) McGowen, J. L.; Ajo, H. M.; Zhang, J. Z.; Schwartz, B. J. Femtosecond studies of hydrated electron recombination following multiphoton ionization. *Chem. Phys. Lett.* 1994, **231**, 504–510.
- (43) Christopher, P.; Xin, H.; Marimuthu, A.; Linic, S. Singular characteristics and unique chemical bond activation mechanism of photocatalytic reactions on plasmonic nanostructures. *Nat. Mater.* 2012, **11**, 1044–1050.
- (44) Sa, J.; Tagliabue, G.; Friedli, P.; Szlachetko, J.; Rittmann-Frank, M. H.; Santomauro, F. G.; Milne, C. J.; Sigg, H. Direct observation of charge separation on Au localized surface plasmons. *Energy Environ. Sci.* 2013, **6**, 3584–3588.
- (45) Pavliuk, M. V.; Fernandes, A. B.; Abdellah, M.; Fernandes, D. L. A.; Machado, C. O.; Rocha, I.; Hattori, Y.; Paun, C.; Bastos, E. L.; Sa, J. Nano-hybrid plasmonic photocatalyst for hydrogen production at 20% efficiency. *Sci. Rep.* 2017, **7**, 8670.
- (46) Antila, L. J.; Santomauro, F. G.; Hammarström, L.; Fernandes, D. L. A.; Sa, J. Hunting for elusive shallow traps in TiO₂ anatase. *Chem. Commun.* 2015, **51**, 10914–10916.
- (47) Guo, X.; Hao, C.; Jin, G.; Zhu, H. Y.; Guo, X. Y. Copper nanoparticles on graphene support: an efficient photocatalyst for coupling of nitroaromatics in visible light. *Angew. Chem., Int. Ed.* 2014, **53**, 1973–1977.